Computational Analysis of Pressure and Wake Characteristics of an Aerofoil in Ground Effect

Stephen Mahon

Xin Zhang

Aerospace Engineering, School of Engineering Sciences, University of Southampton, Southampton SO17 1BJ, UK

The pressure and wake of an inverted cambered aerofoil in ground effect was studied numerically by solving the Reynolds-averaged Navier-Stokes equations. Efforts were focused on the setting up of an accurate numerical model and assessing the abilities of various turbulence models in capturing major physical features associated with the flow, such as surface pressure distribution, separation, level of downforce, and wake. A number of ride heights were studied covering various force regions. Surface pressures, sectional forces, and wake characteristics were compared to experimental data. The $k-\omega$ SST and Realizable $k-\varepsilon$ turbulence models were found to offer good overall simulations, with the $k-\omega$ SST performing better for the surface pressure and the Realizable $k-\varepsilon$ better for the wake. The simulations at various ride heights correctly captured the trends in flow-field variations with ride height. The surface pressures, wake flow field, and region of separation on the suction surface of the aerofoil, at lower ride heights, were all modeled accurately. [DOI: 10.1115/1.1891152]

1 Introduction

Aerodynamics of wings in ground effect has applications to high-performance racing cars. The understanding of flow physics is a relatively recent experience led by wind tunnel model experiments. Despite efforts by various workers, there remain a number of areas deserving further attention [1]. Because of the high cost of wind tunnel model tests, numerical modeling of the flow should be developed and the best practice assessed.

Computational investigations into inverted wings in ground effect started in the 1980s. The earliest work was done by Katz [2] in which a single-element wing in ground effect was modeled using a panel method. Ground effect was modeled using the image-plane method. The method does not take into account viscous effects, and as a result, no downforce reduction at low ride heights was observed.

In engineering applications, numerical solutions of Reynolds-averaged Navier-Stokes (RANS) equations, often in steady state, are generally obatined. The work by Ranzenbach and Barlow [3,4] studied two-dimensional (2D) aerofoils in ground effect. In Ref. [3], a NACA 0015 aerofoil at zero angle of attack was studied. The Reynolds number based on the chord was 1.5×10^6. A RANS solution was sought with the effect of turbulence modeled by a variant of the $k-\varepsilon$ model. The multiblock fully structured grids contained a total of 20,000–30,000 grid points. Force coefficients were compared to tests. In Ref. [4], a cambered airfoil (NACA 4412) was employed. Again the angle of attack was zero and the Reynolds number was 1.5×10^6. In all cases the the ground was stationary, thus, producing a ground boundary layer and an inaccurate ground plane simulation. The downforce compared well to experimental data, obtained by Ranzenbach and Barlow, for a stationary ground case. The results indicated a sharp reduction in downforce at ride heights of the order of 0.05 of the chord. Because of the presence of a thick ground boundary layer, this phenomena, referred to as the force-reduction phenomena, was attributed to the merging of the aerofoil and ground boundary layers.

Recently in a series of studies into an inverted wing in ground effect, Zerihan and Zhang [1] and Zhang and Zerihan [5] highlighted major physical features of wings in ground effect. A study was performed in order to establish a numerical model [6]. The method used solutions of Reynolds-averaged Navier-Stokes equations with turbulence modeled by the Spalart-Allmaras model [7] and the $k-\omega$ SST model [8]. Fully structured grids were used containing up to 30,000 grid points. The results were compared to measured surface pressures and velocities taken at the center of a wing span in ground effect. Major features of the flow were captured. The results yielded good qualitative trends for the aerodynamic performance, using the one-equation model when the surface pressures were compared at different ride heights. In general, the wake thickness was predicted reasonably well in the region near the trailing edge. Further downstream, the wake was predicted to be thicker than that found in the experiments, with reduced velocities. A boundary layer along the ground plane, indicated by the experimental results, was predicted well using the one-equation model, but was significantly too thick using the two-equation model. In all cases a moving ground was simulated.

In another study, Lawson et al. [9] conducted a numerical study of a GA(W)-1 aerofoil in ground effect through solutions of the RANS equations on a fully structured grid. The total number of grid points were 48,500. Turbulence was modeled by the Spalart-Allmaras model [7]. The computational results were compared to experimental surface pressures and particle image velocimetry (PIV) images obtained with a finite wing. A moving ground was simulated in all computational and experimental cases. The agreement between the experimental and computational data was poor because of different values of freestream velocity employed in the experimental and computational studies, thus assuming zero scaling effects. Although the surface pressures were presented, the computational force variations with ride height were not.

The computational studies conducted thus far have contributed to the general understanding of flow physics and, in some cases, supported critical experimental observations. However, few numerical simulations have obtained entirely satisfactory prediction with a moving ground. Agreement with measurements vary

Contributed by the Fluids Engineering Division for publication in the JOURNAL OF FLUIDS ENGINEERING. Manuscript received by the Fluids Engineering Division January 21, 2004. Revised manuscript received September 27, 2004. Review conducted by H. Johari.

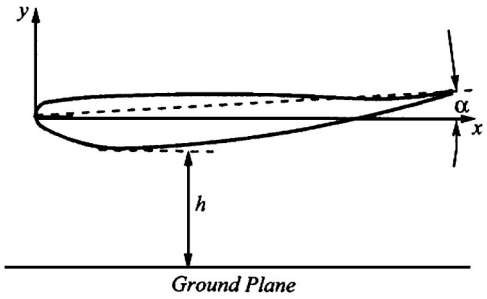

Fig. 1 Definition of the terms and coordinate system

among various studies. The differences can be attributed to various factors, chief among them are type of grid, grid resolution, and turbulence models employed with the RANS simulation. However, there have been no comparative studies between the performance of different turbulence models. The current study aims to investigate the influence of individual turbulence models, using a RANS simulation and wind-tunnel measurements. Although the flow field of a wing in ground effect is inherently three-dimensional, the center-span flow field has been shown to be quasi-two-dimensional [1]. Within this study only two-dimensional cases will be considered in order to decompose the complex flow field generated by a wing in ground effect and obtain a correct computational method without the additional considerations of wing-tip vortices. The focus of this investigation is on both pressures and the wake flow field, since practice dictates that other aerodynamic components follow the front wing of a racing car.

2 Numerical Method

2.1 Aerofoil Geometry and Flow Condition. The aerofoil used in this investigation is a derivative of the LS(1)-0413 MOD profile. A detailed listing of the profile can be found in Zerihan [10]. The aerofoil is inverted such that the suction surface is closest to the ground. The chord c and incidence α of the aerofoil are 223.4 mm and +3.6 deg, respectively. The profile possesses a finite trailing edge of $0.007c$. The ride height h is defined as the vertical distance between the lowest point on the suction surface of the aerofoil and the ground plane. The origin of the coordinates is at the leading edge of the aerofoil (Fig. 1). Incidence, defined as the angle between the chord of the aerofoil and the horizontal, is positive for a nose-down rotation.

All computations were performed at a Reynolds number of 4.6×10^5, with a freestream velocity of 30 m/s. These conditions correspond to the experimental conditions [1,5].

2.2 Governing Equations. Simulations were performed using a RANS solver and were calculated on a linux-based cluster. The numerical solver was set up in a steady-state 2D segregated configuration, which utilized an implicit formulation. In such a configuration solutions at each iteration were obtained by solving the Reynolds-averaged Navier-Stokes equations

$$\frac{\partial \overline{u_j}}{\partial x_j} = 0 \tag{1}$$

$$\frac{\partial}{\partial t}(\rho\overline{u_i}) + \frac{\partial}{\partial x_j}(\rho\overline{u_i u_j}) = -\frac{\partial \overline{p}}{\partial x_i} + \frac{\partial}{\partial x_j}(\overline{\tau_{ij}} - \rho\overline{u_i' u_j'}) \tag{2}$$

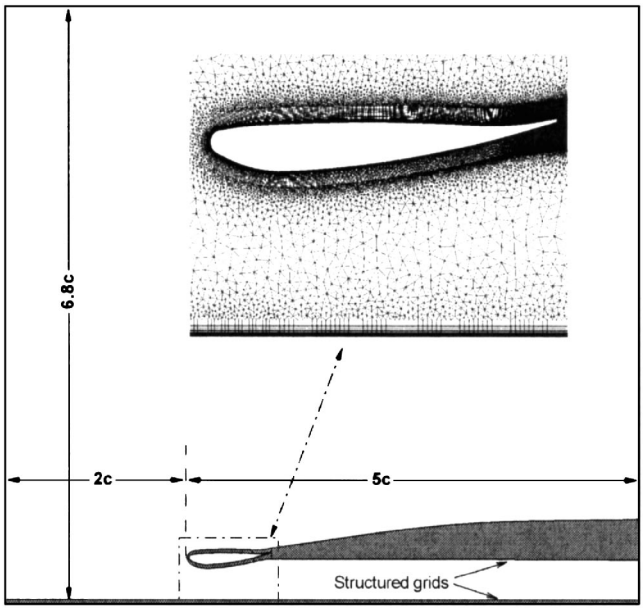

Fig. 2 Schematic of computational domain

$$\frac{\partial}{\partial t}(\rho c_p \overline{T}) + \frac{\partial}{\partial x_j}(\rho c_p \overline{T}\overline{u_j}) = \frac{\partial \overline{p}}{\partial t} + \overline{u_j}\frac{\partial \overline{p}}{\partial x_j} + \overline{u_j'\frac{\partial p'}{\partial x_j}} + \frac{\partial}{\partial x_j}\left(k\frac{\partial \overline{T}}{\partial x_j} - \rho c_p \overline{T' u_j'}\right) + \overline{\Phi} \tag{3}$$

where

$$\overline{\tau_{ij}} = \mu\left(\frac{\partial \overline{u_i}}{\partial x_j} + \frac{\partial \overline{u_j}}{\partial x_i}\right) \tag{4}$$

and

$$\overline{\Phi} = \overline{\tau_{ij}\frac{\partial u_i}{\partial x_j}} \tag{5}$$

An upwind discretization scheme was used for all flow variables, which yielded second-order spatial accuracy. The SIMPLEC pressure-velocity coupling algorithm was used. To aid the rate of convergence V-Cycle and flexible multigrid schemes were used for pressure and momentum, respectively.

The criteria for convergence was specified using the sectional forces of the aerofoil, in particular, C_L. Typically, simulations were run until steady-state values of downforce and drag were observed.

2.3 Turbulence Models. The six turbulence models investigated are the one-equation Spalart-Allmaras model [7], the standard $k-\varepsilon$ model [11], the standard $k-\omega$ model [12], the $k-\omega$ SST model [8], the $k-\varepsilon$ RNG model [13], and the Realizable $k-\varepsilon$ model [14]. Enhanced wall treatments are used with the $k-\varepsilon$ model and corresponding variants.

2.4 Computational Grids. A multiblock hybrid grid design was used, containing both structured and unstructured blocks. At various ride heights, the relative grid topology and structure were maintained. A schematic of the computational domain and grid is shown in Fig. 2. To capture the boundary layer of the aerofoil accurately, a hyperbolically extruded structured grid was used. A conventional structured block was used to capture the ground boundary layer. A separate structured block was positioned directly downstream of the aerofoil with the purpose of capturing the wake. The remainder of the computational domain was unstructured and refined in areas of importance. Within the ground

and aerofoil boundary layer blocks the initial cell spacing, normal to the wall, was set such that $y^+ \approx 1$. The exact number of cells vary according to the ride height. Typically the grids contained of the order of 350,000 cells with the majority of those located toward the trailing edge of the aerofoil and within the wake block.

The boundary conditions were configured to replicate the experimental conditions. The upstream boundary was modeled using a velocity inlet boundary condition. The corresponding inlet velocity was set at 30 m/s in a positive streamwise direction with a uniform vertical distribution. The downstream boundary was modeled using a pressure-outlet boundary condition. The gage pressure was set at zero. The height of the upper edge of the domain above the simulated ground plane corresponded to the height of the wind-tunnel test section. A slip wall boundary condition was imposed on the upper edge therefore imposing a zero cross-flow condition and removing the requirement of additional boundary layer resolution. This formulation was set in order to replicate the experimental conditions imposed by the roof of the wind-tunnel test section.

The aerofoil and ground plane were modeled as solid walls with a no-slip condition enforced. In addition, the ground surface was provided with a translational velocity equal to free stream. In order to model the transition of the aerofoil boundary layers to turbulent, a laminar zone was used within the boundary layer domain, extending downstream from the leading edge to $x/c = 0.1$, in accordance with the experimental data [1]. The streamwise location of the aerofoil is shown in Fig. 2 and was set as a result of a sensitivity study, which was performed prior to conducting the final simulations.

Initial levels of turbulence within the flow were prescribed via values of turbulence intensity and turbulent viscosity ratio. The freestream turbulence intensity level within the 2.1 m $\times$ 1.7 m wind tunnel facility is 0.3% at a freestream velocity of 30 m/s. A turbulent viscosity ratio of 10 was used. Further details concerning the design of the moving ground facility within the 2.1 m $\times$ 1.7 m wind-tunnel facility may be found in the work of Burgin et al. [15].

Fine grids were used in this study to isolate other features of the numerical simulation. A grid sensitivity study was performed at a ride height of $h/c = 0.224$. Three grids were constructed: a coarse grid of 250,000 cells, a medium grid of 350,000 cells, and a fine grid of 450,000 cells. The medium grid was the one eventually used in the study. The variations in grid density were focused in the wing boundary layer block and wake block. Turbulence was modeled with the Realizable $k-\varepsilon$ model. The surface pressures and wake profiles at $x/c = 1.2$ are presented in Fig. 3. Very little variation in the results was observed.

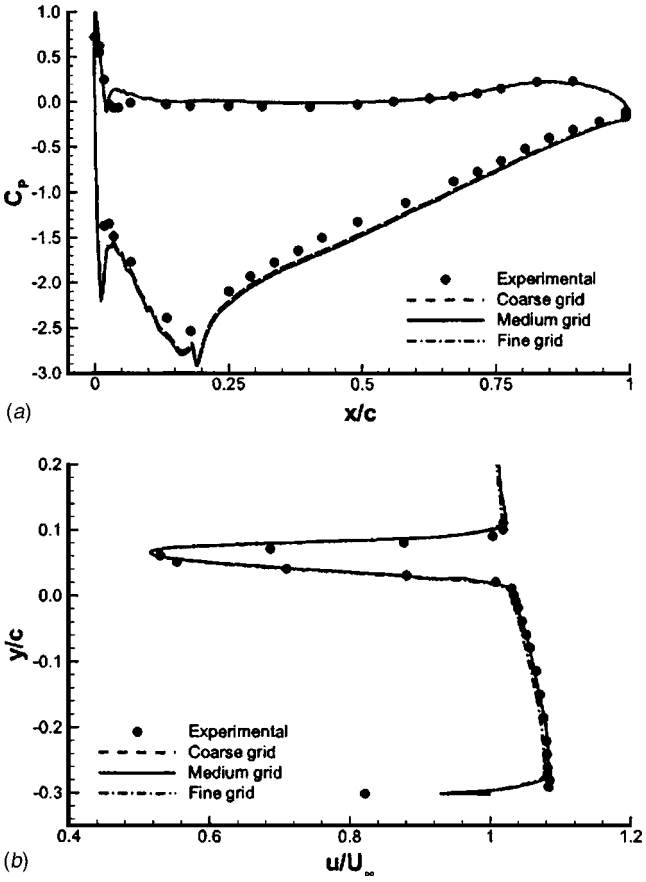

Fig. 3 Effect of grid density: (*a*) surface pressure distributions and (*b*) wake profiles at $x/c = 1.2$

3 Results and Discussion

3.1 Turbulence Models. A quantitative study of turbulence models was conducted. Two cases were selected ($h/c = 0.224$ and 0.09). $h/c = 0.224$ represents a typical flow condition where the ride height of the aerofoil is in the force enhancement region [1], but separation is starting to appear on the suction surface near the trailing edge. At $h/c = 0.09$ a large separation region is present on the suction surface. The suitability of each turbulence model was quantitatively assessed using the surface flow features and wake characteristics.

At $h/c = 0.224$ (Fig. 4(*a*)), all the turbulence models captured the general features of the surface pressures. The leading edge stagnation pressure ($C_{P\text{stag}}$) was accurately predicted at 1.00 by all the turbulence models at $x/c = 0.003$ on the pressure surface. Discrepancies were observed in the prediction of the suction peak ($C_{P\text{suc}}$) and subsequent pressure recovery along the suction surface. The term *suction peak* refers to the value of maximum suction. No single turbulence model captured the entire surface pressure distribution perfectly. However, specific features were captured accurately with various models. At this ride height ($0.224c$) the surface pressures were most accurately predicted with the $k-\omega$ SST model. The quantitative features of the surface pressures predicted by each turbulence model are listed in Table 1.

Comparisons between the numerical and experimental wake data at $x/c = 1.2$ are also presented in Fig. 4(*b*). The experimental wake profile was measured by Zhang and Zerihan [5] using the laser Doppler anemometry (LDA) technique in a separate wind-tunnel study. Unlike the surface pressures a wide variation in the prediction of the wake profile was observed. It may be noted that toward the ground plane the nondimensional velocity (u/U_∞) decreases to approximately 0.89 then sharply increases to a value of unity. Since the ground plane is provided with a freestream velocity this trend seems incorrect. However, it must be remembered that the aerofoil generates an adverse streamwise pressure gradient because of the recovery of the flow beneath the suction surface. This, in turn, generates a boundary layer along the ground plane originating from a streamwise location corresponding to the suction peak. The resulting ground boundary layer velocity profile is present at all ride heights and is accordingly present in all the computational wake profiles.

The standard $k-\varepsilon$ model failed to capture the vertical location of the lower boundary of the wake (δ_{bottom}) and the corresponding velocity recovery, resulting in an unrealistic velocity profile. The standard $k-\omega$, $k-\omega$ SST, and Spalart-Allmaras models all captured the velocity deficit ($u_{\min}$) accurately, however, they failed to accurately predict the velocity recovery at the lower wake boundary. The $k-\varepsilon$ RNG and Realizable $k-\varepsilon$ models provided accurate predictions of the lower boundary, however, the $k-\varepsilon$ RNG model underpredicted the velocity deficit. The most accurate prediction of the wake profile was obtained with the Realizable $k-\varepsilon$ model,

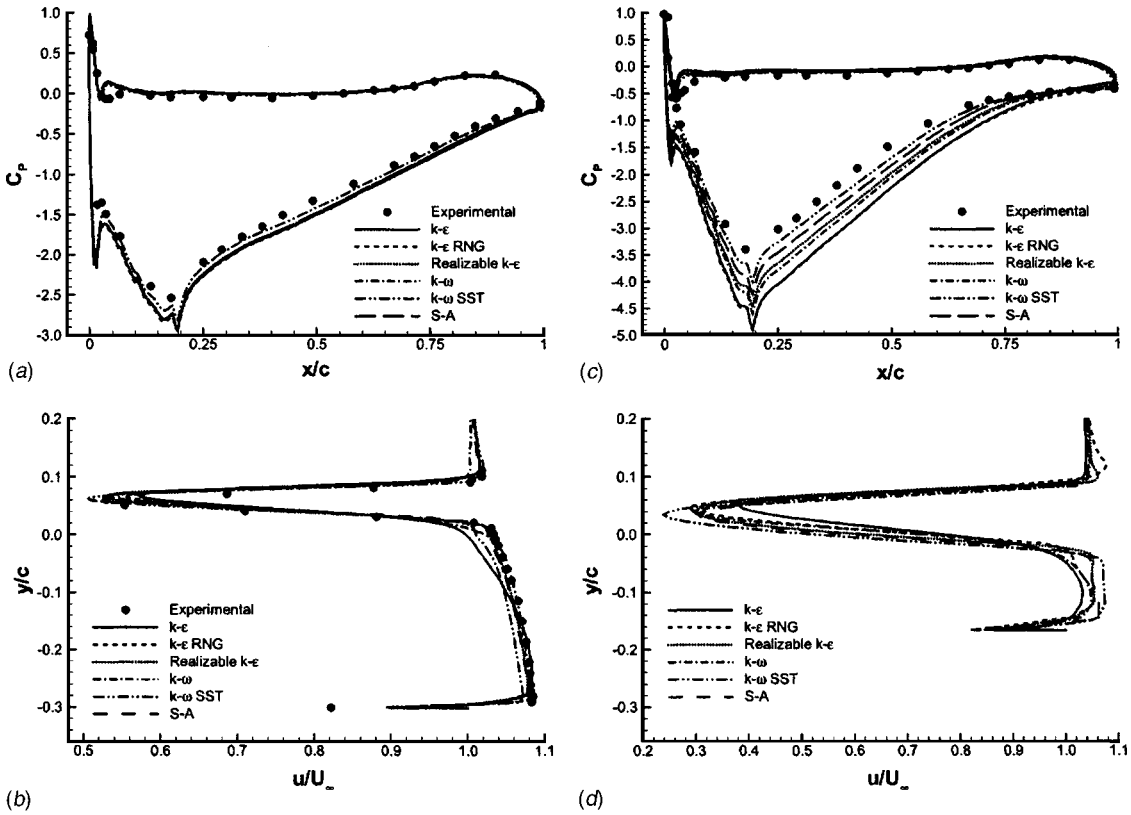

Fig. 4 Effects of turbulence models: (*a*) surface pressures at $h/c=0.224$, (*b*) wake profiles at $x/c=1.2$ for $h/c=0.224$, (*c*) surface pressures at $h/c=0.09$, and (*d*) wake profiles at $x/c=1.2$ for $h/c=0.09$

which correctly predicted the velocity deficit, wake thickness, and corresponding boundaries. Table 2 lists quantitative data concerning the wake profiles predicted by each turbulence model.

At $h/c=0.09$ (Fig. 4(*c*)), separation occurs well ahead of the trailing edge and poses an additional challenge to the numerical model. The surface pressures again suggest that the $k-\omega$ SST model gives the best prediction, with the variation between turbulence models observed at the higher ride height amplified. There are no wake measurements at this height, but we note that the variations between the turbulence models were similar to those observed at the higher ride height (Fig. 4(*d*)).

Table 1 Surface pressure information for various turbulence models, $h/c=0.224$

Turbulence model	$C_{P\text{suc}}$	x/c at $C_{P\text{suc}}$
Experimental	−2.53	0.18
Spalart-Allmaras	−2.92	0.19
Standard $k-\omega$	−2.92	0.19
$k-\omega$ SST	−2.81	0.19
Standard $k-\varepsilon$	−2.94	0.19
$k-\varepsilon$ RNG	−2.97	0.19
Realizable $k-\varepsilon$	−2.92	0.19

3.2 Surface Pressures. We now proceed to investigate the effect of ride height, using the $k-\omega$ SST and the Realizable $k-\varepsilon$ models. Calculations were performed at $h/c=0.448$, 0.313, 0.224, 0.179, 0.134, 0.112, and 0.09. Quantitative data concerning the general flow field, surface pressures, wake characteristics, and sectional forces was extracted.

The calculated surface pressures and the experimentally measured values are shown in Fig. 5. Only two heights are included for clarity. The agreement between the computational and experimental pressures on the pressure surface of the aerofoil was good. The leading edge stagnation point was accurately predicted at $x/c=0.003$ for all ride heights with both turbulence models. As the ride height was reduced, discrepancies were observed in the pressure surface pressures between $x/c=0.024$ and 0.134, where the pressures were overpredicted. This was attributed to a spike in the curvature of the aerofoil at $x/c=0.016$, which resulted in a

Table 2 Wake information for various turbulence models at $x/c=1.2$ and $h/c=0.224$

Turbulence model	$u_{\min}/U_\infty$	y/c at $u_{\min}$	y/c at δ_{top}	y/c at δ_{bottom}	δ_{99}/c
Experimental	0.53	0.06	0.09	0.02	0.07
Spalart-Allmaras	0.55	0.07	0.10	0.02	0.08
Standard $k-\omega$	0.53	0.07	0.10	0.01	0.09
$k-\omega$ SST	0.51	0.06	0.09	0.02	0.07
Standard $k-\varepsilon$	0.57	0.07	0.10	0.01	0.09
$k-\varepsilon$ RNG	0.56	0.07	0.10	0.02	0.08
Realizable $k-\varepsilon$	0.53	0.07	0.09	0.02	0.07

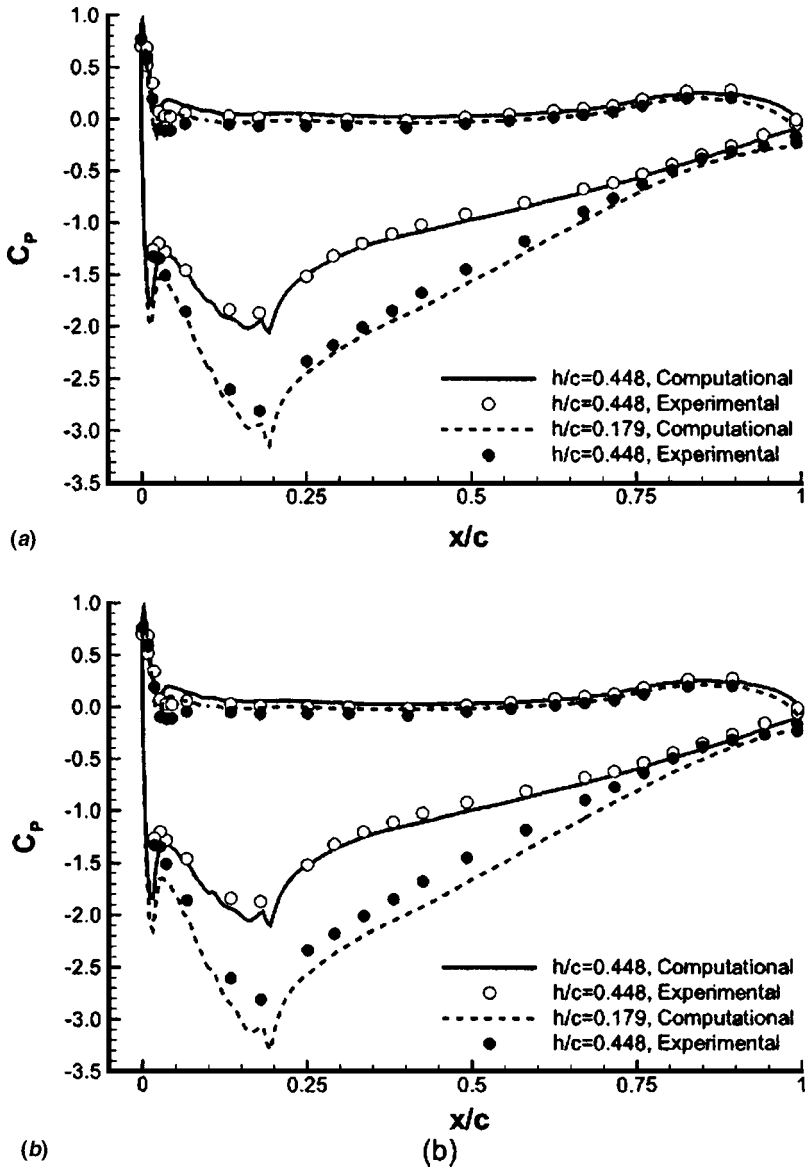

Fig. 5 Surface pressures at various ride heights: (*a*) $k-\omega$ SST model and (*b*) Realizable $k-\varepsilon$

sudden deceleration in the flow. The experimental data illustrated a gradual increase in C_P within this region, possibly because of the spike in curvature being absent, due to manufacturing techniques.

The suction surface pressures were slightly overpredicted with the overprediction increasing with decreasing ride height. A suction spike was observed at $x/c=0.013$, the magnitude of which increased as the simulated ride height was reduced. This leading edge suction spike was not observed in the experiment because of the discrete nature of the surface pressure data. Directly downstream of the the leading edge suction peak, a decrease in suction was observed at $x/c=0.023$. The curvature of the aerofoil at this location was discontinuous, resulting in a region of decelerated flow. Disturbances in the suction surface pressures between $x/c=0.033$ and $x/c=0.180$ were observed, corresponding to yet more discontinuities in the curvature.

The suction surface peak was consistently observed at $x/c=0.190$, increasing in magnitude with decreasing ride height. The suction peak was overpredicted for all ride heights. Downstream of the suction peak existed a region of pressure recovery extending to the trailing edge. The rates at which the pressures recovered along the suction surface were accurately captured for all nondimensional ride heights with the $k-\omega$ SST model. The Realizable $k-\varepsilon$ model, however, overpredicted the pressure recovery rate at $h/c=0.09$ resulting in an inaccurate finite pressure difference at the trailing edge.

Overall the $k-\omega$ SST model gives a better prediction at all heights, especially lower ride heights mainly in the pressure recovery region on the suction surface. The pressures on the pressure surface experience relative small variations over the range of heights.

3.3 Sectional Forces. The sectional forces generated by the aerofoil at various ride heights are shown in Fig. 6. The predicted downforce is compared to the sectional values measured experimentally. The overall trend in downforce variation was captured most accurately with the $k-\omega$ SST model. The Realizable $k-\varepsilon$ model overpredicted the downforce at all ride heights and failed to accurately predict the stall of the aerofoil. There is a marked improvement with the $k-\omega$ SST model because of better prediction of the pressure recovery process. As mentioned previously, the suction surface pressures were overestimated for all ride heights,

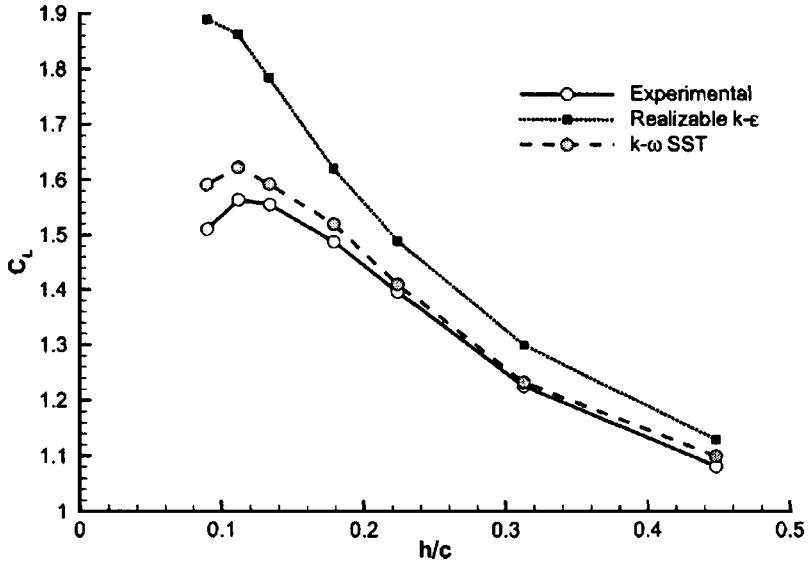

Fig. 6 Sectional forces at various ride heights

accordingly the calculated values of downforce were also overestimated. This feature is particularly acute near the maximum downforce ride height. The largest discrepancy occurs at the maximum force height of $h/c=0.112$. At this ride height the value of downforce (C_L) predicted by the $k-\omega$ SST model is 2% greater than the measured value and for the Realizable $k-\varepsilon$ model 19% greater. The reduction in downforce at $h/c=0.09$ due to the aerofoil stalling [1] was correctly predicted with the $k-\omega$ SST model whereas the Realizable $k-\varepsilon$ failed to predict the stall.

3.4 Flow Between Aerofoil and Ground. Figure 7 presents line contours of nondimensional streamwise velocity (u/U_∞) for $h/c=0.448$ and 0.09. The contours for $h/c=0.448$ show a slightly accelerated flow beneath the aerofoil and a thin wake. A small region of recirculation was observed directly downstream of the finite trailing edge. Decreasing the ride height caused the flow beneath the wing to become increasingly accelerated with maximum values of $u/U_\infty=2.0$ achieved at $h/c=0.09$.

The contours of u/U_∞ indicated that the flow located between

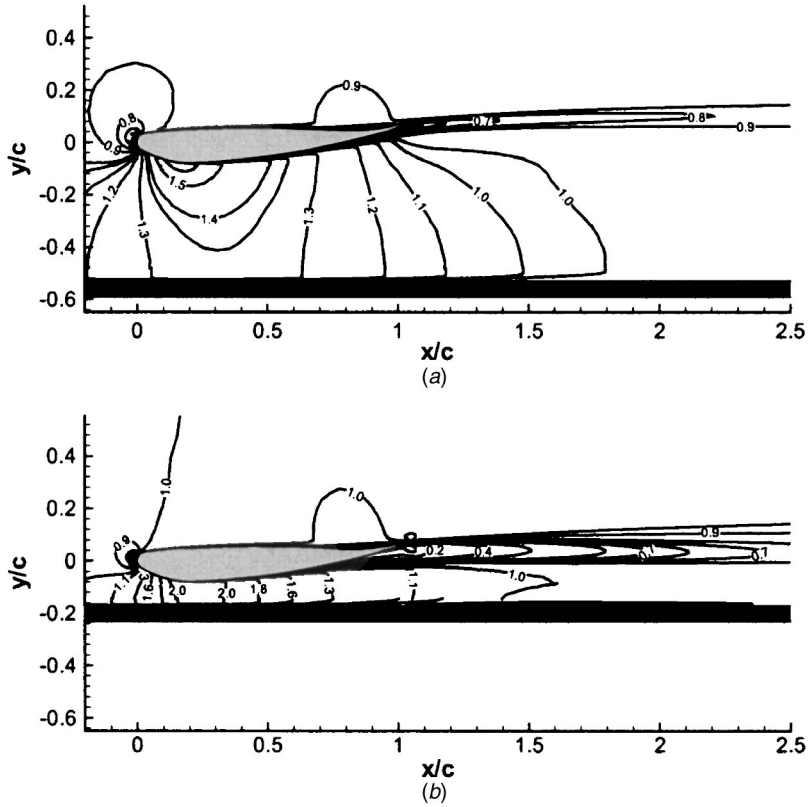

Fig. 7 Contours of u/U_∞ with the Realizable $k-\varepsilon$ model: (*a*) $h/c=0.448$ and (*b*) $h/c=0.09$

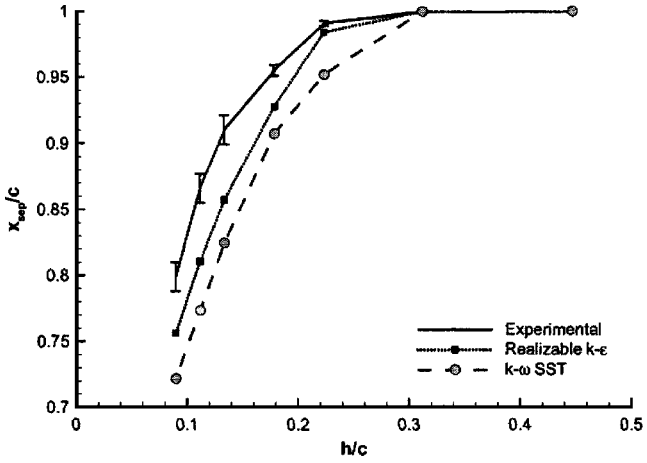

Fig. 8 Streamwise location of separation for various ride heights

the lower boundary of the wake and ground possessed higher than freestream values of velocity. This region of flow was seemingly constrained by the lower boundary of the wake, forming a wall jet. Decreasing the ride height caused the wall jet to become increasingly accelerated, a trend that was observed experimentally [5].

Figure 8 shows the streamwise location of separation (x_{sep}/c) on the suction surface of the aerofoil. The measured values for a wing with free transition [1] are also included since values with fixed transition were not available. The location of separation moved upstream along the suction surface as the ride height was decreased, a trend that was observed in both experiment and computation. This was a direct result of the pressure gradient beneath the aerofoil becoming increasingly adverse as the ride height was reduced. When compared to the experimental separation locations the computed values were overpredicted for all ride heights even though the surface pressures indicated good agreement. This overprediction was attributed to the difference in the location of transition on the suction surface of the aerofoil between the experimental and computational data. Transition was found to occur naturally at $x/c=0.3$ to 0.35 [1], whereas, within this study and for all other experimental data, transition was fixed at $x/c=0.1$. Accordingly, the suction surface boundary layer will be thicker at a fixed streamwise location for the fixed transition case, therefore, more prone to separation. A quantitative comparison concerning the location of separation can therefore not be made because of the difference between experimental and computational setup.

3.5 Wake Flow Field. The turbulent wake downstream of the aerofoil is seen in Fig. 7. The size of the wake increases as the ride height is reduced. The development of the wake is constrained by the ground. As the ride height is reduced and the wall jet is formed by the boundary layer separation on the suction surface and the ground, the lower boundary of the wake changes. The velocity deficit in the wake increases as the ride height is reduced. Further downstream the velocity deficit was slowly recovered, which is accompanied by an increase in the thickness of the wake.

Figure 9 shows the profiles of relative streamwise velocity, tangential to the ground plane at a streamwise locations of $x/c=1.2$. Only three ride heights are included in the figure, corresponding to ride heights with available experimental data. A summary of the prediction is given in Table 3.

Unlike the surface pressure prediction where the $k-\omega$ SST model gives the best prediction, the Realizable $k-\varepsilon$ model produces the most accurate prediction of the wake profile. Both turbulence models accurately predicted the velocity deficit within the ground boundary layer, associated thickness, and the thickening thereof with reducing ride height. The velocity deficit within the wake and top wake boundary were also predicted well by both models, however, discrepancies were observed within the prediction of the lower wake boundary. The $k-\omega$ SST model underpredicted the rate of velocity recovery toward the lower wake boundary, resulting in an slightly inaccurate prediction of the lower wake boundary, and an overprediction in the wake thickness. The Realizable $k-\varepsilon$ model accurately predicted the lower wake boundary and the corresponding rate of velocity recovery. Accordingly the wake thickness was accurately predicted by the Realizable $k-\varepsilon$ model.

4 Further Comments

Accurate, realistic steady-state computations of an inverted aerofoil in ground effect were obtained, quantifying the effects of grid resolution, turbulence model, and ride height. A strong dependence of the surface pressures over the suction surface of the aerofoil on ride height was observed. The channel created between the suction surface of the aerofoil and the ground plane resembles a Venturi nozzle. The flow entering between the leading edge and the ground plane is therefore initially accelerated until the throat of the nozzle (the lowest point on the aerofoil suction surface), then decelerated underneath the downstream section of the aerofoil. The rate of acceleration and deceleration is dependent on the shape of the nozzle and hence the ride height, with low ride heights generating greater velocities. The surface pressures illustrate this process with reductions in ride height generating suction surface pressures of greater magnitude, while the pressure surface pressure remain relatively constant. The streamwise location of the suction peak was independent of ride height at $x/c=0.190$, corresponding to the throat of the channel and, therefore, the location of highest velocity. The surface pressures obtained in the study show improvement over earlier efforts. The $k-\omega$ SST model was found to offer the best prediction of the surface pressures over the entire range of ride heights, from the force-enhancement region to force-reduction region [1].

At high ride heights the accelerated flow underneath the aerofoil could recover to a freestream value prior to the aerofoil trailing edge. Reducing the ride height created a velocity recovery rate, which could not be physically achieved. Therefore, a flow that possessed a greater-than-freestream value of velocity such that $\overline{u}/U_\infty > 1.0$, was generated, i.e., a wall jet.

The flow beneath the aerofoil exists into a region constrained by the ground plane and the lower wake boundary. Unlike the surface pressures and sectional forces the Realizable $k-\varepsilon$ model was found to produce the best prediction of the wake flow. A jet flow between the lower boundary of the wake and the ground plane was observed, especially at low ride heights ($h/c=0.09$). It is well documented that flows with large mean strain rates, such as jets, are difficult to model using turbulence models. The method adopted by the Realizable $k-\varepsilon$ model is to calculate the eddy viscosity locally therefore allowing the model to remain realizable even in regions of large mean strain rates. Shih et al. [14] has shown that this modification results in a much improved simulation of jet flows, in particular, the spreading rates. It could, therefore, be hypothesised that improved simulations of the ground jet flow resulted in improved simulations of the lower boundary of the wake and hence the entire wake flow.

It was noted that the thickness of the wake increased as the ride height decreased. However the transverse location of the upper boundary of the wake remained constant at $y/c \approx 0.15$, i.e., the transverse location of the lower boundary of the wake decreases with ride height. It has been shown that as the ride height is decreased, the magnitude of the wall jet increases. It is felt that the downward translation of the lower wake boundary with decreasing ride height is linked to the strength of the wall jet, however, conclusions cannot be drawn without further investigation.

The numerical investigations conducted were two-dimensional, whereas in reality the flow field generated by a wing in ground

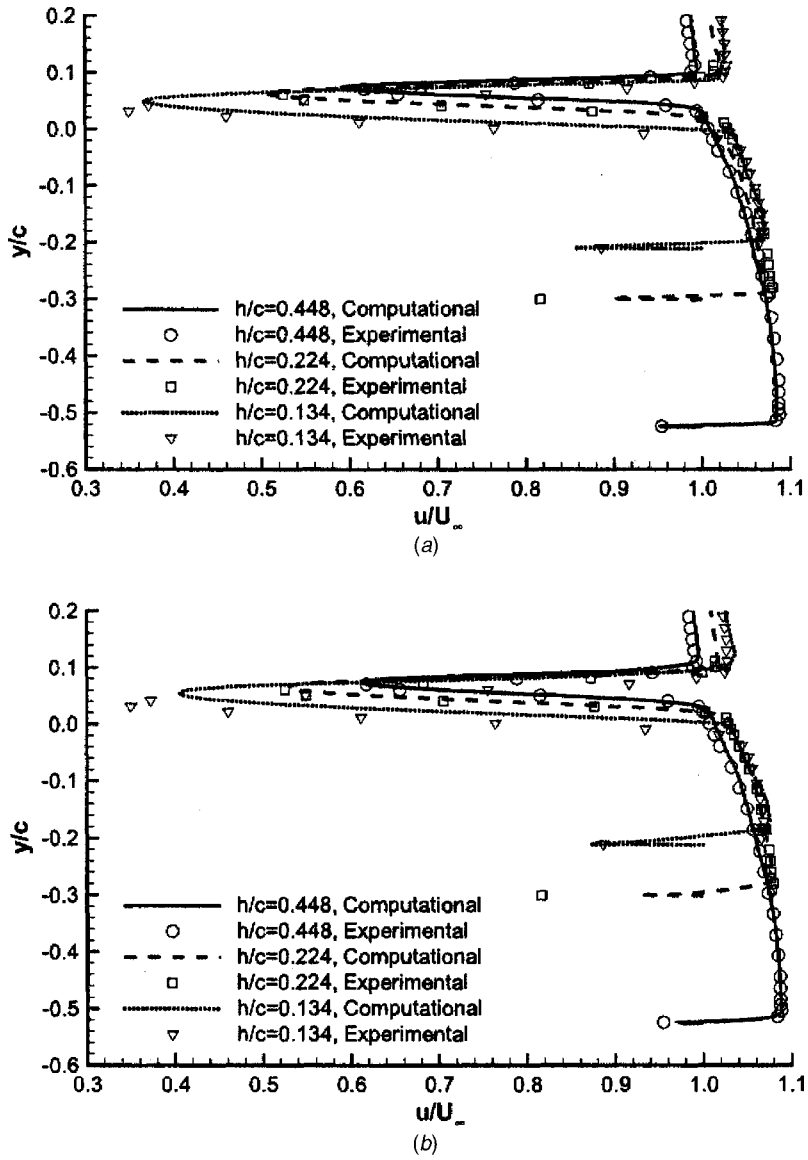

Fig. 9 Wake profiles at $x/c=1.2$: (*a*) $k-\omega$ SST and (*b*) Realizable $k-\varepsilon$

effect is intrinsically three-dimensional. Within this study the performance of each turbulence model was based on the two-dimensional values of surface pressures and wake flow field. Within a three-dimensional case, the performance of numerical schemes will, in addition, be based on the predictive capability concerning the wing tip vortices. More complex schemes, such as large eddy simulation (LES) and detached eddy simulation (DES), may therefore be more suited to the situation of a wing in ground effect due to the good predictive capabilities concerning vortical flows.

Table 3 Wake information for various ride heights at $x/c=1.2$

h/c	Expt/CFD	u_{min}/U_∞	y/c at u_{min}	y/c at δ_{top}	y/c at δ_{bottom}	δ_{99}/c
0.448	Expt	0.617	0.071	0.103	0.032	0.071
	Real $k-\varepsilon$	0.613	0.074	0.110	0.004	0.106
	$k-\omega$ SST	0.591	0.073	0.099	0.037	0.062
0.224	Expt	0.525	0.061	0.090	0.022	0.068
	Real $k-\varepsilon$	0.529	0.065	0.098	0.024	0.074
	$k-\omega$ SST	0.507	0.063	0.091	0.022	0.069
0.134	Expt	0.350	0.031	0.082	−0.016	0.098
	Real $k-\varepsilon$	0.405	0.054	0.094	0.004	0.090
	$k-\omega$ SST	0.367	0.049	0.085	−0.001	0.086

5 Conclusion

A numerical investigation into an aerofoil in ground effect was undertaken. The effects of turbulence model, grid density, and ride height were all investigated, and the following conclusions may be drawn:

1. The two-dimensional flow field generated by an inverted aerofoil in ground effect can be accurately modeled by solving the Reynolds-averaged Navier-Stokes equations.
2. The most accurate predictions of the surface pressures and sectional forces were obtained with the $k-\omega$ SST turbulence model.
3. The most accurate predictions concerning the wake flow field, in particular, the lower wake boundary, were obtained with the Realizable $k-\varepsilon$ turbulence model. The formulation of this turbulence model provided improved predictions of the wall jet and hence improved simulations of the lower wake boundary.

Acknowledgments

The authors would like to thank BARf1 for their continuing support and help. In particular, the authors would like to thank Jonathan Zerihan and Willem Toet for their input and technical discussion.

Nomenclature

c = chord
C_L = sectional lift coefficient, $L/q_\infty c$
C_p = coefficient of pressure, $(p-p_\infty)/q_\infty$
$C_{P\text{stag}}$ = coefficient of pressure at the leading edge stagnation point
$C_{P\text{suc}}$ = coefficient of pressure at maximum suction
h = ride height
L = lift, positive indicates downforce i.e. force in a negative y direction
p = static pressure
q_∞ = dynamic head, $\frac{1}{2}\rho U_\infty{}^2$
t = time
u,v,w = streamwise, traverse and spanwise velocity components
$\overline{u}$ = mean streamwise velocity at $x/c=1$ between the lower trailing edge and the ground plane
$u_{\min}$ = minimum u velocity component in wake
U_∞ = freestream velocity
x,y = Cartesian coorinates, x positive downstream, y positive upward
x_{sep} = suction surface separation point
y^+ = nondimensional length, yU_τ/v

Greek Symbols

α = incidence of aerofoil, positive for a nose down rotation
δ_{bottom} = bottom of wake thickness
δ_{top} = top of wake thickness
δ_{99} = wake thickness as measured by 99% displacement thickness
μ = viscosity
ρ = density

Subscripts

∞ = freestream

References

[1] Zerihan, J. D. C. and Zhang, X., 2000, "Aerodynamics of a Single Element Wing in Ground Effect," J. Aircr. **37**(6), pp. 1058–1064.
[2] Katz, J., 1985, "Calculation of the Aerodynamic Forces on Automotive Lifting Surfaces," ASME J. Fluids Eng. **107**, pp. 438–443.
[3] Ranzenbach, R. and Barlow, J. B., 1994, "Two-Dimensional Airfoil in Ground Effect, An Experimental and Computational Study," SAE Paper No. 94-2509.
[4] Ranzenbach, R. and Barlow, J., 1996, "Cambered Airfoil in Ground Effect: An Experimental and Computational Study," SAE Paper No. 96-0909.
[5] Zhang, X. and Zerihan, J. D. C., 2003, "Off-Surface Aerodynamic Measurements of a Wing in Ground Effect," J. Aircr. **40**(4), pp. 716–725.
[6] Zerihan, J. D. C. and Zhang, X., 2001, "A Single Element Wing in Ground Effect: Comparisons of Experiments and Computation," AIAAPaper 2000-0423, pp. 1–12.
[7] Spalart, P. R. and Allmaras, S. R., 1992, "A One-Equation Turbulence Model for Aerodynamic Flows," AIAA Paper No. 92-0439.
[8] Menter, F. R., 1994, "Two-Equation Eddy-Viscosity Turbulence Models for Engineering Applications," AIAA J. **32**(8), pp. 1598–1605.
[9] Lawson, N. J., Knowles, K., Hart, R. J. E., Wray, J. N., and Eyles, J. M., 2002, "An Experimental Investigation Using PIV of the Underflow of a GA(W)-1 Aerofoil Section in Ground Effect," *Proc. of the 4th MIRA International Vehicle Aerodynamics Conference, 16-17 October*, MIRA, Warwick, pp. 1–14.
[10] Zerihan, J. D. C., 2001. "An Investigation Into the Aerodynamics of Wings in Ground Effect," Ph.D. thesis, University of Southampton, Southampton, UK.
[11] Launder, B. E. and Spalding, D. B., 1974. "The Numerical Computation of Turbulent Flows," Comput. Methods Appl. Mech. Eng. **3**, pp. 269–289.
[12] Wilcox, D. C., 1988, "Multiscale Models for Turbulent Flows," AIAA J. **26**(11), pp. 1311–1320.
[13] Yakhot, A. and Orszag, S., 1986, "Renormalisation Group Analysis of Turbulence: I Basic Theory," J. Sci. Comput. **1**(1), pp. 1–51.
[14] Shih, T-H, Liou, W. W, Shabbir, A., Yang, Z., and Zhu, J., 1995, "A New $k-\epsilon$ Eddy Viscosity Model for High Reynolds Number Turbulent Flows," Comput. Fluids **24**, pp. 227–238.
[15] Burgin, K., Adey, P. C., and Beatham, J. P., 1986, "Wind Tunnel Tests on Road Vehicle Models Using a Moving Belt Simulation of Ground Effect," J. Wind. Eng. Ind. Aerodyn. **22**, pp. 227–236.